Conformation of an Endogenous Ligand in a Membrane Bilayer for the Macrophage Scavenger Receptor CD36[†]

Xin-Min Li,[‡] Robert G. Salomon,[§] Jun Qin,[∥] and Stanley L. Hazen*[,‡,⊥]

Department of Cell Biology, Department of Molecular Cardiology, Department of Cardiovascular Medicine, and Center for Cardiovascular Diagnostics and Prevention, Cleveland Clinic Foundation, Cleveland, Ohio 44195, and Department of Chemistry, Case Western Reserve University, Cleveland, Ohio 44106

Received January 25, 2007; Revised Manuscript Received March 1, 2007

ABSTRACT: Phagocytic removal of aged or oxidatively damaged cells and macromolecules is an indispensable homeostatic function of the innate immune system. A structurally conserved family of oxidized phospholipids that serve as endogenous high-affinity ligands for the macrophage scavenger receptor CD36 ($oxPC_{CD36}$) was recently identified. Enriched within atherosclerotic plaque and senescent cell membranes, $oxPC_{CD36}$ promote the uptake of oxidized lipoproteins and cell membranes by macrophages when present at only a few molecules per particle. How macrophages recognize $oxPC_{CD36}$ within cellular membranes and lipoprotein surfaces remains unknown. Herein, we deduce the conformation of $oxPC_{CD36}$ near the hydrophobic−hydrophilic interface within membrane bilayers by determining multiple critical internuclear distances using nuclear Overhauser enhancement spectroscopy. The molecular model reveals a unique conformation for $oxPC_{CD36}$ within bilayers whereby the distal end of the sn-2 acyl chain harboring the structurally conserved CD36 recognition motif protrudes into the aqueous phase. The remarkable conformation elucidated for $oxPC_{CD36}$ produces a surface accessible phagocytic "eat me signal" to facilitate senescent cell and oxidized lipoprotein recognition by the scavenger receptor CD36 as part of its immune surveillance function.

Accurate and dependable recognition of oxidatively modified lipoproteins and senescent or apoptotic cells by macrophages is essential to a diverse number of physiological processes ranging from resolution of inflammation to tissue remodeling and immune cell selection (*1*−*5*). Mediated by numerous receptors (*6*−*11*), the scavenger receptor CD36 has emerged as an important contributor to phagocytic recognition, engulfment, and clearance of apoptotic and senescent cells in vivo (*6*, *7*, *9*, *11*−*14*). Moreover, the scavenger receptor CD36 has also been implicated in the atherosclerotic process because of its ability to both recognize oxidized forms of low-density lipoprotein (LDL) and facilitate cholesterol accumulation and macrophage foam cell formation, the first cellular hallmark of the atherosclerotic process (*6*, *15*, *16*).

We previously discovered a novel family of structurally specific oxidized phosphatidylcholine molecular species that serve as high-affinity ligands for CD36 ($oxPC_{CD36}$)[1] (*17*, *18*). A common structural motif for $oxPC_{CD36}$ species was identified as an oxidatively truncated *sn*-2 acyl group with a terminal γ-hydroxy (or oxo) α,β-unsaturated carbonyl (Figure 1a). Mass spectrometry analyses revealed that $oxPC_{CD36}$ are generated by a variety of physiological oxidation processes (*18*) and are enriched in both atherosclerotic plaques and senescent or effete cell membranes (*17*, *19*). Recent studies similarly identified structurally analogous oxPS species that are generated during apoptosis, which together with $oxPC_{CD36}$ serve as critical participants in macrophage recognition of apoptotic cells via the scavenger receptor CD36 (*20*). Moreover, cellular and animal model studies demonstrate an essential role for oxPC−CD36-mediated intracellular signaling via JNK and ERK pathways during macrophage foam cell formation in vivo (*21*). Changes in the organization of lipids can have profound effects on both cellular functions and disease processes (*22*). The structure of CD36 lipid ligands within biomembranes and modified lipoprotein surfaces is thus of interest in further understanding the involvement of macrophage CD36 in both

[†] This research was supported by National Institutes of Health Grants HL70621, P01 HL076491, P01 HL077107, HL081064, and HL53315.

* To whom correspondence should be addressed: Center for Cardiovascular Diagnostics and Prevention, 9500 Euclid Ave., NE-10, Cleveland Clinic, Cleveland, OH 44195. Telephone: (216) 445-9763. Fax: (216) 636-0392. E-mail: hazens@ccf.org.

[‡] Department of Cell Biology and Center for Cardiovascular Diagnostics and Prevention, Cleveland Clinic Foundation.

[§] Case Western Reserve University.

[∥] Department of Molecular Cardiology, Cleveland Clinic Foundation.

[⊥] Department of Cardiovascular Medicine, Cleveland Clinic Foundation.

[1] Abbreviations: DMPC, dimyristoylphosphatidylcholine (also 14:0,14:0 PC); DMPC-d_{67}, 1,2-dimyristoyl-d_{54}-*sn*-glycero-3-phosphocholine-1,1,2,2-d_4-*N*,*N*,*N*-trimethyl-d_9; DPPC-d_{75}, 1,2-dipalmitoyl-d_{62}-*sn*-glycero-3-phosphocholine-1,1,2,2-d_4-*N*,*N*,*N*-trimethyl-d_9; KOdiA-PC,1-palmitoyl-2-(5-keto-6-octenedioyl)phosphatidylcholine; MLV, multilamellar vesicles; NMR, nuclear magnetic resonance spectroscopy; NOE, nuclear Overhauser enhancement spectroscopy; oxLDL, oxidized low-density lipoprotein; oxPC, oxidized phosphatidylcholine; $oxPC_{CD36}$, oxPCs that bind to the scavenger receptor CD36; POPC, 1-palmitoyl-2-oleoylphosphatidylcholine (also 16:0,18:1 PC); SUV, small unilamellar vesicles; TDNOE, truncated driven nuclear Overhauser enhancement spectroscopy; TOCSY, total (homonuclear) correlated spectroscopy; 14:0 LPC, 1-myristoyllysophosphatidylcholine; 18:1,18:1 PE, dioleoylphosphatidylethanolamine.

10.1021/bi700163y CCC: $37.00
Published on Web 04/04/2007

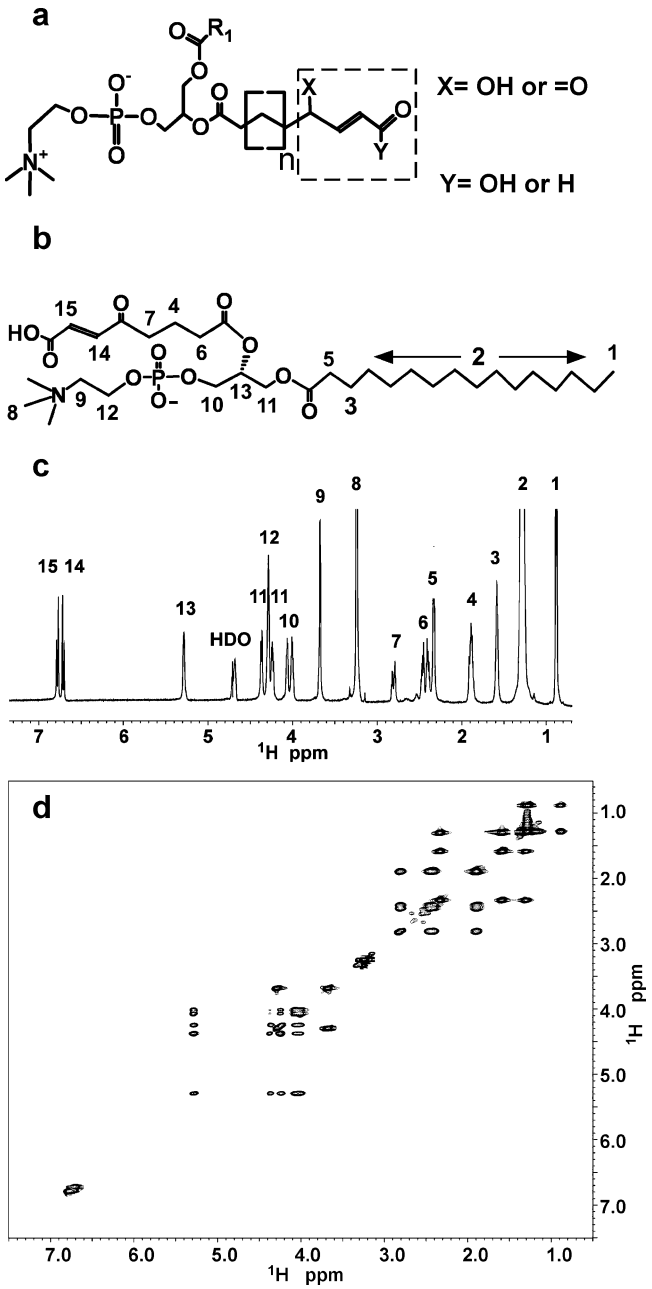

FIGURE 1: (a) Structure of oxPC$_{CD36}$. The length of the oxidized truncated *sn*-2 acyl chain varies depending upon the parent (unoxidized) fatty acid precursor, where $n = 2$, 3, and 7 for docosahexanoic acid, arachidonic acid, and linoleic acid, respectively. The structural motif within the dashed box confers high-affinity CD36 recognition when tethered to the *sn*-2 acyl group of a phospholipid (*17*, *18*). (b) Structure of 1-palmitoyl-2-(5-keto-6-octenedioyl)phosphatidylcholine (KOdiA-PC), a prototypic oxPC$_{CD36}$, along with (c) the conventional 800 MHz ^{1}H NMR spectrum with peak assignments for KOdiA-PC. (d) 2D TOCSY spectrum of KOdiA-PC with a mixing time of 60 ms. KOdiA-PC was prepared by extrusion in 20 mM sodium phosphate buffer and 100 mM NaCl in D_2O (pD 7.4).

normal immune surveillance recognition and potential pathological processes such as atherosclerosis.

Nuclear Overhauser enhancement spectroscopy (NOESY), in both the solid state and the solution phase, has been widely used to study the structure and dynamics of lipids (*23*−*30*). These studies typically involve either homogeneous bulk phase classes of lipids, individual molecular species of phospholipids, or defined binary or higher-complexity combinations of phospholipid/sterol mixtures. As far as we are aware, however, no studies to date have examined the conformation of an endogenous low-abundance structurally defined molecular species of oxidized phospholipid within a sea of fluid phase phospholipid matrix. Herein, we report the first conformational analysis for a lipid ligand of a scavenger receptor within a membrane bilayer. Using solution nuclear Overhauser enhancement (NOE) spectroscopy, multiple critical internuclear (through-space) distances were determined for a stable and structurally specific oxPC ligand for CD36 within model membrane bilayers. A remarkable membrane conformation of the endogenous lipid ligand for CD36 is identified, providing structural insights into how macrophages use CD36 to recognize senescent or apoptotic cells and modified lipoproteins as part of normal homeostatic surveillance functions. They also provide a structural platform for the rational development of potential therapeutic strategies for blocking macrophage recognition of oxidized lipoproteins and foam cell formation during atherogenesis.

EXPERIMENTAL PROCEDURES

Materials. 1-Palmitoyl-2-(5-keto-6-octenedioyl)phosphatidylcholine (KOdiA-PC) was purchased from Cayman Chemical (Ann Arbor, MI). 1,2-Dimyristoyl-d_{54}-*sn*-glycero-3-phosphocholine-1,1,2,2-d_4-*N*,*N*,*N*-trimethyl-d_9 (DMPC-d_{67}), 1-*O*-1′-(*Z*)-octadecenyl-2-oleoyl-*sn*-glycero-3-phosphocholine (18:0,18:1 plasmenylcholine), 1,2-dipalmitoyl-d_{62}-*sn*-glycero-3-phosphocholine-1,1,2,2-d_4-*N*,*N*,*N*-trimethyl-d_9 (DPPC-d_{75}), and other lipids were obtained from Avanti Polar Lipids (Alabaster, AL). All other chemicals were of the highest available quality and purchased from Sigma (St. Louis, MO).

Vesicle Preparation. Appropriate amounts of phospholipids were initially dissolved in $CDCl_3$, mixed, and dried with N_2 prior to being exhaustively dried under vacuum overnight. To prepare SUV, lipids were initially fully hydrated by addition of buffer [20 mM phosphate buffer and 100 mM NaCl in D_2O (pD 7.4) or 50 mM Hepes buffer and 100 mM NaCl in a 1:1 D_2O/H_2O mixture (pH 7.0) for ^{31}P NMR] in argon-purged sealed vials above the phase transition temperature. Following vortexing to disperse the hydrated lipids, SUV were generated by extrusion through 0.4 μm (six times) and then 0.1 μm polycarbonate filters (11 times) using an Avanti Mini-Extruder Set (Avanti Polar Lipids). Throughout all the experiments, freshly prepared vesicles were maintained well above the phase transition temperature to avoid vesicle fusion. The hydrodynamic radius of SUV preparations was determined with a DynaPro-801 dynamic light scattering instrument with MicroCell attachment and Dynamics 4.0 (Protein Solutions Inc., Charlottesville, VA). The performance of the instrument was verified with polystyrene bead standards and a 2 mg/mL aqueous solution of bovine serum albumin prior to sample measurement.

Before NMR studies, dynamic light scattering was used to determine particle size and size distribution. The mean liposome diameter of the vesicles comprised of either 100 mol % DMPC or 100 mol % POPC was 100 ± 5 or 80 ± 2 nm, respectively. The mean liposome diameter of the vesicles comprised of either 20 mol % KOdiA-PC and 80 mol % DMPC or 20 mol % 18:0,18:1 plasmenylcholine, 20 mol % KOdiA-PC, and 60 mol % DMPC was 68 ± 4 nm.

The intensity-weighted size distributions of KOdiA-PC-containing vesicles showed one apparent narrow population of particles, indicating the vesicles were small and uniform.

NMR Experiments. All lipids and lipid dispersions were freshly prepared and kept under an inert atmosphere (either Ar or N_2) in sealed NMR tubes. ^{31}P NMR measurements were performed by using a Varian Inova 600 MHZ spectrometer at 242.85 MHz. The chemical shift positions of lipid dispersions were recorded relative to 85% H_3PO_4 (0 ppm). All ^{1}H NMR experiments were carried out on Bruker Avance 600 or 800 MHz spectrometers equipped with cryogenic probes at 30 °C. Two-dimensional (2D) NOE spectra were recorded in the phase-sensitive mode. Short mixing times (200, 150, 100, and 50 ms) were used in the 2D NOESY experiments to minimize spin diffusion effects. Spectra were processed using NMRPipe (*31*). TDNOE experiments were performed as described by Wager and Wüthrich (*32*), with 600 scans for one-dimensional (1D) NOE difference spectra. As previously reported for liposome systems, the correlation time can be assumed to remain constant (*24*, *27*, *33*, *34*), and the approximate distances (r) between protons were obtained from the initial buildup rate (σ) of the NOE according to the following equation (*35*):

$$r_{ij}/r_{kl} = (\sigma_{kl}/\sigma_{ij})^{1/6} \quad (1)$$

The known distance between α- and β-vinyl ether protons of 18:0,18:1 plasmenylcholine (2.3 Å) was used as an internal reference with which to estimate internuclear distances via comparison of their first-order NOE initial buildup rates. Only the initial linear regions of the buildup rate curves were used for rate calculations. We observed that when using the vinyl ether proton buildup rate to calculate the distance between choline protons in the same sample [i.e., the $N(CH_3)_3$ and penultimate methylene ($N\text{-}CH_2$) protons] in multiple distinct PC-containing samples of varied SUV composition, the distance calculated between these choline protons was always similar. We therefore used this distance and buildup rate for calculations in the few samples in which the plasmalogen was not included (some specimens with concomitant inclusion of cholesterol in the SUV). Because lateral diffusion effects in lipid dispersions are inevitable (*36*−*38*), care was taken to ensure initial buildup rates for estimation of the internuclear distances were used only during the period that is short relative to the rate of spin diffusion of the liposome system, as reported previously (*23*, *24*, *27*, *33*, *39*). The structure illustrated for KOdiA-PC was generated using CS Chem3D Ultra (version 10.0), while ensuring agreement between the observed NOE distances and the corresponding distances in the structural model.

RESULTS

^{1}H NMR Peak Assignments for Oxidized Lipids. To probe the conformation of $oxPC_{CD36}$ within membrane bilayers, we incorporated synthetic 1-palmitoyl-2-(5-keto-6-octenedioyl)-phosphatidylcholine (KOdiA-PC), a prototypic $oxPC_{CD36}$ species, within model membranes comprised of perdeuterated dimyristoyl-PC. KOdiA-PC (structure, Figure 1b) is one of the most potent and chemically stable $oxPC_{CD36}$ and is enriched within atherosclerotic plaques (*17*, *18*). Recent studies also demonstrate that KOdiA-PC can confer CD36-specific recognition, macrophage cholesterol accumulation, and foam cell formation when present at <5 mol % within membrane bilayers or modified lipoproteins (*17*). Initial examination of KOdiA-PC by both ^{1}H NMR and two-dimensional total (homonuclear) correlation spectroscopy (TOCSY) (Figure 1c,d) confirmed substantial differences in chemical shifts of protons present in distinct regions of the molecule, including the proximal and distal portions of both *sn*-1 and *sn*-2 aliphatic chains, the glycerol backbone, and the polar headgroup (chemical shift assignments shown in Figure 1b). These results suggested that proton NMR-based interrogations of KOdiA-PC in model membranes might thus be able to provide information sensitive to the environment throughout multiple regions of the $oxPC_{CD36}$ molecule.

Evidence Supporting a Lamellar (Bilayer) Mesophase in Model Membranes Containing $oxPC_{CD36}$ Using ^{31}P NMR. Because lipid dispersions can adopt alternative mesomorphic phases, before proceeding with conformational analyses we felt it important to probe how incorporation of $oxPC_{CD36}$ species impacts the bilayer (lamellar) phase of model membranes. ^{31}P NMR of phospholipids is sensitive to both the dynamics and organization of model and biological membranes and may thus help distinguish between lipid mesomorphic phases (*40*, *41*). The ^{31}P NMR method is a well-recognized approach and has been frequently used both to monitor the characteristics of the lamellar phase for lipid systems (*42*−*44*) and to estimate vesicle size (*45*). The ^{31}P NMR spectrum of KOdiA-PC (data for 20 mol % shown; similar results were observed with 5 mol %) incorporated into DMPC vesicles demonstrated an axially symmetric isotropic peak, indicating rapid rotational averaging of the chemical shift tensor around the membrane normal, a characteristic of small unilamellar vesicles (SUV) (Figure 2a). Data supporting the notion that KOdiA-PC incorporated into DMPC vesicles retained a lamellar (bilayer) packing structure were obtained by demonstrating ^{31}P NMR spectra (chemical shift, line width, and line shape) similar to those obtained with SUV comprised of either POPC or DMPC, known lamellar phase-preferring phospholipids at the temperatures that were studied (*40*, *44*). In contrast, comparisons with the ^{31}P NMR spectra observed with alternative mesomorphic phase-preferring hydrated lipid dispersions demonstrate marked differences [e.g., micelle-preferring lipids such as lysophosphatidylcholine demonstrated a typical narrow isotropic peak with a half-height line width of 4 Hz; hexagonal array-preferring lipids like phosphatidylethanolamine species exhibited a high-field shoulder and a low-field peak, and multilamellar vesicles exhibited a low-field shoulder and a high-field peak (Figure 2a)].

The Terminal End of the Oxidized Truncated sn-2 Fatty Acid of KOdiA-PC Is in Spatial Proximity to the $N(CH_3)_3$ Choline Protons in Model Membranes, As Determined by 2D NOE. While NOE has been widely used in determining molecular structure and internuclear distances within both small molecules and proteins in solution (*46*), its use in aqueous solutions of membrane vesicles has been limited due to the slow molecular motions, line broadening, and loss of spatial information with traditional steady state NOE techniques. However, monitoring the kinetics of resonance intensity buildup with TDNOE has proven useful in determining internuclear distances within membrane vesicles because effects from spin diffusion are minimized (*24*, *27*, *33*). Further, use of SUV generated with a small radius of

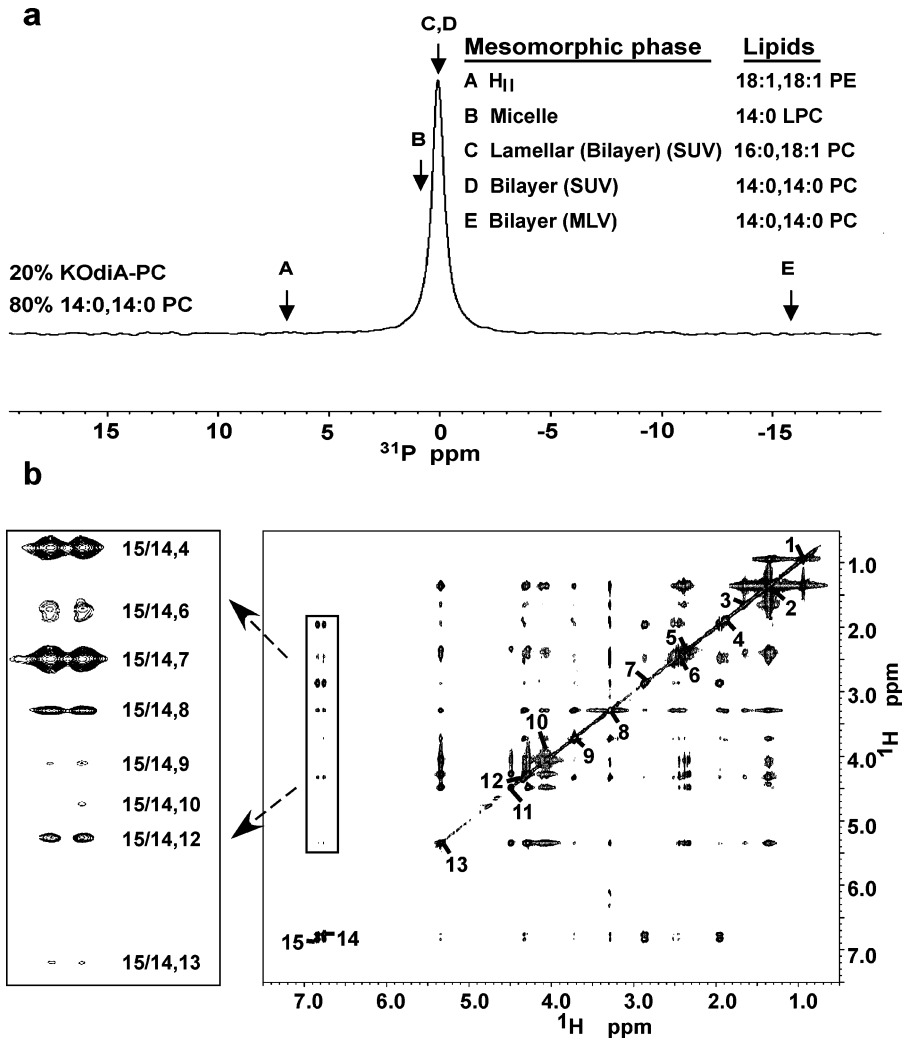

FIGURE 2: (a) ^{31}P NMR spectra of SUV comprised of 20 mol % KOdiA-PC and 80 mol % DMPC (14:0,14:0 PC). Vertical arrows indicate the peak resonances on ^{31}P NMR spectra of distinct mesomorphic phase lipid standards: (A) hexagonal array (H_{II}), dioleoylphosphatidylethanolamine (18:1,18:1 PE); (B) micelle, 1-myristoyllysophosphatidylcholine (14:0 LPC); (C) lamellar (SUV bilayer), 1-palmitoyl-2-oleoylphosphatidylcholine (16:0,18:1 PC) or (D) dimyristoylphosphatidylcholine (14:0,14:0 PC); and (E) MLV bilayers, 14:0,14:0 PC. (b) 2D NOE contour plot of 20 mol % KOdiA-PC and 80 mol % DMPC-d_{67} in phosphate buffer (pD 7.4) recorded at 30 °C. The experiment was carried out in a phase-sensitive mode with a mixing time of 200 ms. Proton chemical shift assignments refer to those illustrated in Figure 1b.

curvature, such as those created via extrusion, permits greater isotropic motion, and hence spectral resolution. Figure 2b is a typical 2D NOE spectrum obtained from KOdiA-PC (20 mol % data shown; NOEs were also observed with 5 mol %) within deuterium-labeled dimyristoyl-PC (DMPC-d_{67}) SUV.

Interrogation of the conformation of $oxPC_{CD36}$ within the model membrane vesicles was facilitated by the fact that KOdiA-PC contains separate and distinct covalent entities throughout the polar headgroup, glycerol backbone, and *sn*-1 and *sn*-2 acyl chains whose different chemical shifts allow for the complete resolution of proton resonances throughout the different regions of the $oxPC_{CD36}$ species. Of interest, multiple protons in the distal *sn*-2 acyl chain demonstrated NOE signals with multiple polar headgroup protons (Figure 2b), indicating close through-space proximity between the terminal end of the *sn*-2 acyl chain and the polar headgroup. For example, intense cross-peaks were observed between the terminal vinyl protons on the truncated *sn*-2 oxidized acyl chain of $oxPC_{CD36}$ (labeled as protons 14 and 15 in Figure 2b; see Figure 1b for structure and proton labeling scheme) and both choline methylene (labeled as protons 9 and 12 in Figure 2b) and terminal methyl [$N(CH_3)_3^+$] groups (labeled as proton 8 in Figure 2b). The NOE between the headgroup and distal *sn*-2 chain protons was still observed with a decrease in mixing time (e.g., 50 ms), and no NOEs were detected between the terminal end of the oxidized truncated *sn*-2 fatty acid (e.g., protons 14 and 15) and the *sn*-1 methylene groups (protons labeled 2 in Figure 1b).

Further 2D NOE examination of KOdiA-PC within DMPC-d_{67} SUV revealed that while NOE signals could be detected between protons of the proximal region of both the *sn*-1 chain (e.g., protons on the α carbon, labeled 5) and *sn*-2 chain (e.g., protons on the α′ and β′ carbons, labeled 6 and 4, respectively; Figure 2b), no NOEs were detected between the protons of the proximal *sn*-1 chain (e.g., protons on the α and β carbon, labeled 5 and 3, respectively) and the protons of the mid and distal *sn*-2 chain (e.g., protons on the γ′carbon and more distal vinyl protons, labeled 7, 14, and 15, respectively). Detection of NOE signals between protons is exquisitely sensitive to distance (eq 1 in Experimental Procedures) and requires a distance between hydrogen

atoms of <5 Å. The results given above thus indicate the spatial proximity between the terminal end of the *sn*-2 acyl chain of $oxPC_{CD36}$ within membrane bilayers and the polar headgroup and support a molecular model in which the oxidized *sn*-2 chain within $oxPC_{CD36}$ extends into the aqueous interface, as opposed to penetrating deep into the hydrophobic core. Consistent with this model, these results also demonstrate an $oxPC_{CD36}$ conformation that possesses a distance of <5 Å between the proximal portions (α and *β* positions) of both *sn*-1 and *sn*-2 acyl chains, but not between the mid and distal *sn*-1 chain and the mid or distal *sn*-2 chain. This conformational model for $oxPC_{CD36}$ is unique for lamellar (bilayer) phase dispersions, since separate experiments with pure (100 mol %) KOdiA-PC showed no evidence of NOE cross-peaks between the terminal vinyl protons on the truncated *sn*-2 oxidized fatty acid (protons 14 and 15 in Figure 2b) and the terminal methyl protons of choline [$N(CH_3)_3^+$]. The reason for this became clear during ^{31}P NMR analyses of 100 mol % KOdiA-PC aqueous dispersions, which demonstrated spectral features consistent with a micellar mesopomorphic phase (isotropic peak at 1 ppm).

Identification of Critical Internuclear Distances between Protons of the Oxidized Truncated sn-2 Fatty Acid of KOdiA-PC and both Glycerol and the Choline Headgroup in Model Membranes. Upon irradiation of resonances in the distal *sn*-2 acyl chain during 1D NOE experiments, multiple polar headgroup protons exhibited NOE signals, indicating close through-space proximity between the terminal end of the *sn*-2 acyl chain and the polar headgroup. To further define the spatial relationships between protons of the polar headgroup and the oxidized *sn*-2 chain of $oxPC_{CD36}$ within membranes, critical internuclear distances were determined using truncated driven 1D NOE (TDNOE). First, the distances between the terminal vinyl protons on the *sn*-2 oxidized acyl chain of $oxPC_{CD36}$ (protons 14 and 15) and the choline terminal methyl [$N(CH_3)_3^+$] protons (labeled 8) were ascertained within KOdiA-PC (20 mol %) incorporated in DMPC-d_{67} SUV. To serve as an internal reference with which to calibrate distances, synthetic 18:0,18:1 plasmenylcholine (20 mol %) was also introduced into the perdeuterated DMPC SUV. Irradiation of these vesicles at 4.3 ppm, which corresponds to the *β*-vinyl ether proton of the plasmalogen, resulted in the subsequent buildup of resonance corresponding to the *sn*-1 α-vinyl ether protons (Figure 3a). Substantial and exponential increases in the resonance intensity buildup in the terminal vinyl protons on the truncated *sn*-2 oxidized acyl chain (protons 14 and 15) were similarly demonstrated during irradiation of vesicles at 3.24 ppm, the chemical shift corresponding to the choline terminal methyl [$N(CH_3)_3^+$] protons of KOdiA-PC (Figure 3a). Using the known distance (2.3 Å) between the α- and *β*-vinyl protons in the *sn*-1 vinyl ether linkage of plasmenylcholine, the distances between other protons were deduced by internal comparisons of their respective initial rate for TDNOE buildup during NOE experiments (eq 1 in Experimental Procedures). The results indicate that the vinyl protons on the terminal *sn*-2 chain (protons 14 and 15) were on average ~3.8 Å from the choline $N(CH_3)_3^+$ protons.

Additional NOE intensity buildup curves between different proton pairs were similarly generated from buildup rates of NOE difference spectra following irradiation of protons in

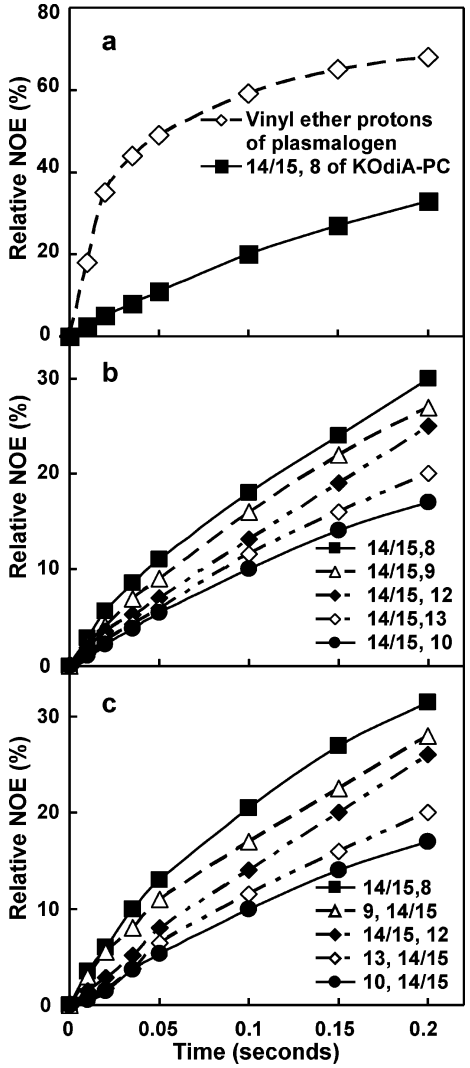

FIGURE 3: TDNOE intensity buildup curves for the NOE difference spectra between the indicated proton pairs in SUV comprised of (a) 20 mol % KOdiA-PC, 20 mol % 18:0,18:1 plasmenylcholine, and 60 mol % DMPC-d_{67}, (b) 20 mol % KOdiA-PC and 80 mol % DMPC-d_{67} at 30 °C, or (c) 20 mol % KOdiA-PC, 50% mol DPPC-d_{75}, and 30 mol % cholesterol at 37 °C: (a) (◇) α- and *β*-vinyl ether proton pair of 18:0,18:1 plasmenylcholine and (■) protons 14 and 15 vs proton 8 of KOdiA-PC, (b) (■) protons 14 and 15 vs proton 8, (△) protons 14 and 15 vs proton 9, (◆) protons 14 and 15 vs proton 12, (◇) protons 14 and 15 vs proton 13, and (●) protons 14 and 15 vs proton 10, and (c) (■) protons 14 and 15 vs proton 8, (△) proton 9 vs protons 14 and 15, (◆) protons 14 and 15 vs proton 12, (◇) proton 13 vs protons 14 and 15, and (●) proton 13 vs protons 14 and 15. For all proton pairs that are listed, the second proton listed was irradiated, and the buildup rate in the first indicated proton resonance(s) monitored during TDNOE. All data points represent three entirely independent preparations.

distinct regions of the $oxPC_{CD36}$ species. These permitted calculation of multiple internuclear distances between the distal end of the *sn*-2 acyl chain of $oxPC_{CD36}$ and other protons throughout the polar headgroup and glycerol backbone of the molecule (Figure 3b). $^1H-^1H$ NOE is mediated by through-space dipolar interactions and thus theoretically might not distinguish between inter- and intramolecular nuclear spin exchange in vesicles. Further, formation of "rafts" of $oxPC_{CD36}$ species within SUV might theoretically occur. However, several lines of evidence suggest that the observed NOEs are intramolecular, and not intermolecular. First, NOE kinetics were investigated over a wide range of

Table 1: NOE-Derived Critical Internuclear Distances of KOdiA-PC within Membrane Bilayers[a]

proton pairs		DMPC	DPPC/cholesterol
9 vs 8	$N\text{-}CH_2/N(CH_3)_3$	3.5 Å	3.5 Å
14 and 15 vs 8	$HC{=}CH/N(CH_3)_3$	3.8 Å	4.0 Å
9 vs 14 and 15	$N\text{-}CH_2/HC{=}CH$	3.3 Å	3.4 Å
14 and 15 vs 12	$HC{=}CH/CH_2OP$	3.4 Å	3.5 Å
10 vs 14 and 15	$g_3/HC{=}CH$	4.2 Å	4.0 Å
10 vs 14 and 15	$g_2/HC{=}CH$	4.3 Å	4.1 Å

[a] Comparison of the internuclear distances of the indicated different proton pairs of KOdiA-PC (20 mol %) incorporated into small unilamellar vesicles comprised of either DMPC-d_{67} (80 mol %) or DPPC-d_{75} and cholesterol (50 and 30 mol %, respectively). Proton number assignments correspond to those indicated in Figure 1. The glycerol backbone protons at the *sn*-2 and *sn*-3 positions are abbreviated as g_2 and g_3, respectively.

$oxPC_{CD36}$ concentrations (even <5 mol %). Performance of the TDNOE experiments within membranes comprised of >75 mol % perdeuterated DMPC dramatically reduced the level of potential nearest neighbor interactions, making the NOE distances measured representative of intra- instead of intermolecular nuclear spin exchange measurements. Indeed, no differences were observed in the initial rates of resonance enhancement in studies with perdeuterated DMPC SUV containing <5 mol % KOdiA-PC versus 20 mol % KOdiA-PC, strongly suggesting their intramolecular character. Further, ^{31}P NMR spectra of the $oxPC_{CD36}$-containing SUV display symmetrical and relatively narrow line widths (Figure 2a). These results indicate that the freshly prepared $oxPC_{CD36}$-containing SUV are experiencing isotropic motion and that the low $oxPC_{CD36}$ mole percent is well mixed within the bulk lipid bilayer and did not form a micelle. The clarity of the solution further suggests that the hydrated lipid dispersions that were analyzed did not form microdomains or aggregates.

Independent Conformation Analyses of KOdiA-PC in Physiological Membranes. In a separate series of 1D and 2D NOE studies, we further investigated the conformation of $oxPC_{CD36}$ in model membranes comprised of more physiological lipid mixtures than DMPC. We incorporated KOdiA-PC at low mole percentages into membranes comprised of binary mixtures of both cholesterol (30 mol %) and perdeuterated DPPC carrier to more closely simulate plasma membrane lipid composition and phospholipid chain length. Like the NOEs observed with KOdiA-PC/DMPC-d_{67} SUV, 2D NOEs of KOdiA-PC in cholesterol/DPPC-d_{75} SUV illustrated intense NOE cross-peaks between the α,β-unsaturated protons on the truncated *sn*-2 oxidized fatty acid (labeled as 14 and 15 protons in Figure 2b) and many protons in the polar headgroup, especially the methyl groups of choline, $N(CH_3)_3^+$ (Figure 2b).

To further compare the spatial relationships between protons of the polar headgroup and the oxidized *sn*-2 chain of $oxPC_{CD36}$ within model membranes comprised of cholesterol and DPPC-d_{75}, critical internuclear distances were again determined using 1D TDNOE experiments and by monitoring the initial buildup rates using short irradiating times. For these studies, rather than addition of synthetic plasmenylcholine as an internal reference for distance calculations as described above, we instead used the distance observed between the choline protons $[N(CH_3)_3]$ and penultimate methylene ($N\text{-}CH_2$), ~3.5 Å (Table 1). This distance is consistent with previous reports for DMPC (*33*), indicating

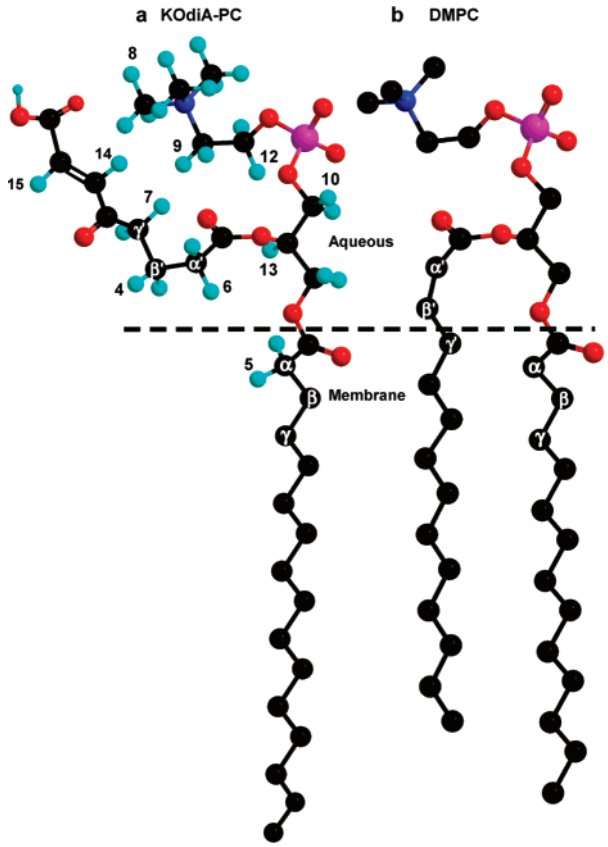

FIGURE 4: Comparison of the structure of lamellar phase phosphatidylcholine (e.g., DMPC) (b) and the predicated conformation of KOdiA-PC within hydrated DMPC or DPPC/cholesterol small unilamellar vesicles (a) near the hydrophobic−hydrophilic interface. The structure illustrated for KOdiA-PC was generated using CS Chem3D Ultra (version 10.0), with agreement between the observed NOE distances and the corresponding distances in the structural model. The conformation of DMPC was built according to reported X-ray diffraction, neutron diffraction, and NMR studies (*47*−*50*).

that there is no significant change for the distance between the choline protons $[N(CH_3)_3]$ and penultimate methylene ($N\text{-}CH_2$) during lipid *sn*-2 acyl chain oxidation. Figure 3C shows the 1D NOE buildup curves of 20% KOdiA-PC/30% cholesterol/50% DPPC-d_{75} SUV for the same proton pairs as previously investigated using 20% KOdiA-PC/80% DMPC-d_{67} SUV. Internuclear distances between critical proton pairs of KOdiA-PC in membranes comprised of either DMPC-d_{67} or cholesterol and DPPC-d_{75} are listed in Table 1. Remarkably similar results were obtained in the distinct membrane systems.

Model of KOdiA-PC in Model Membranes. As a reference point against which the conformation of KOdiA-PC in model membranes will be compared, Figure 4b illustrates the previously published conformation of DMPC in hydrated membranes based upon X-ray diffraction, neutron diffraction, and NMR studies (*47*−*51*). Figure 4a illustrates a molecular model showing the spatial proximity between the vinyl protons on the terminal end of the *sn*-2 acyl chain of KOdiA-PC within a membrane bilayer and the various protons of the choline polar headgroup and glycerol backbone, as computed from TDNOE data. Several unique features of the conformation of KOdiA-PC in model membranes are deduced from these studies. Our NMR results support a solution structure in which the first (carbonyl) and second (α') carbons of the *sn*-2 acyl chain of KOdiA-PC within membranes have

a conformation similar to that of DMPC (Figure 4). However, the remainder of the *sn*-2 acyl chain demonstrates conformations significantly different from that of DMPC, with many protons on the *sn*-2 chain being in the spatial proximity of the polar headgroup choline $N(CH_3)_3^+$ protons. Notably, the α carbon proton (proton 5) on the *sn*-1 acyl chain of KOdiA-PC in bilayers demonstrates no detectable NOE with the γ' proton (proton 7) of the *sn*-2 acyl group, indicating a through-space internuclear distance of >5 Å (Figure 4). In marked contrast, for DMPC in bilayers, these protons are ~3.7 Å apart (*47*). Taken together, these results suggest that conformations of KOdiA-PC in membrane bilayers are on the whole consistent with a molecular model for $oxPC_{CD36}$ in which the proximal portion of the *sn*-2 acyl chain is markedly bent with the distal end protruding completely into the aqueous phase (Figure 4).

DISCUSSION

A cornerstone of molecular and cellular biology is the fluid mosaic model of cell membranes (*52*). An integral feature of this model is the macromolecular assembly of amphipathic phospholipids into a bilayer structure, with polar headgroups directed toward the aqueous phase, and hydrophobic aliphatic fatty acid chains at the *sn*-1 and *sn*-2 positions of phospholipids extending toward the membrane interior. The membrane architecture posited in the fluid mosaic model explains how individual phospholipids and proteins can diffuse rapidly throughout the two-dimensional surface of the membrane; however, a classic bilayer structure does not readily explain how a macrophage scavenger receptor like CD36 can identify senescent or apoptotic cells via the presence of low-abundance structurally specific oxidized phospholipids interspersed within a membrane bilayer. The studies presented here suggest that endogenous oxidized phospholipids, like KOdiA-PC, may instead adopt markedly different conformations, with their peroxidized *sn*-2 fatty acid chains protruding into the aqueous phase, rather than pointing inward which is typical within the hydrophobic membrane interior with nonoxidized aliphatic chains. This novel global conformation for *sn*-2 oxidized fatty acids within phospholipids may thus help explain how a macrophage scavenger receptor like CD36 can identify senescent or apoptotic cells, or a modified lipoprotein.

At physiological temperatures, membranes are highly dynamic structures, with considerable motion of both acyl chain and polar headgroup moieties of phospholipids within their respective hydrophobic and aqueous phases, yet only a single structure is illustrated for KOdiA-PC within a membrane bilayer in Figure 4. The distances measured by NOE in these studies represent an overall average of available conformations. The model shown thus serves as an illustration of one of many (the average) possible conformations of KOdiA-PC and conforms to the general notion of the *sn*-2 oxidized fatty acid group protruding at the surface whereby it remains relatively close to the choline headgroup.

Lipid peroxidation of membrane lipids is accompanied by addition of numerous polar moieties on fatty acid chains. If it is sufficiently polar, thermodynamic forces no doubt drive the conformation toward one directly visualized in the case of KOdiA-PC within a membrane bilayer, a prototypic member of the $oxPC_{CD36}$ family. Thus, as cell membranes and lipoproteins age and undergo oxidation, if not remodeled through the actions of phospholipases, they may "grow whiskers" comprised of an assortment of protruding oxidized *sn*-2 fatty acids of varied structures. The subset that possesses the correct high-affinity structural motif to serve as pattern recognition ligand for the macrophage receptor CD36, $oxPC_{CD36}$, may thus facilitate macrophage recognition and engulfment. Other phospholipid-tethered oxidized fatty acid species may in turn serve as recognition ligands for alternative receptors. Macrophages are continuously "tasting" their environment, extending pseudopodia in search of targets possessing structurally specific "eat me signal" that trigger phagocytosis; in the case of CD36, a terminal γ-hydroxy (or oxo) α,β-unsaturated carbonyl is required on the tip of the oxidatively truncated *sn*-2 acyl group (Figure 1a). It is interesting to note that comparisons among the various $oxPC_{CD36}$ demonstrate a general trend for those possessing longer acyl chain lengths having greater binding affinity for CD36 (*17*−*19*), consistent with an enhanced ability of the *sn*-2 chain to extend into the aqueous phase for CD36 recognition.

Lipid peroxidation is an integral and inexorable process within aerobic respiring organisms, occurring in biological processes ranging from aging itself to inflammation and immune host defenses. Macrophages perform a critical homeostatic function of innate immunity, by accurately and dependably (*33*) recognizing biologic targets for phagocytic engulfment and clearance that have become oxidatively "damaged" through inflammation or have undergone cellular senescence or apoptosis. The recent discovery of a structurally conserved family of oxidized phospholipids that serve as endogenous high-affinity ligands for the scavenger receptor CD36 suggested their role as a novel lipidic eat me signal for macrophage-mediated corpse clearance and oxidized lipoprotein engulfment (*17*−*19*). Biological targets having undergone lipid peroxidation by multiple distinct oxidative pathways become enriched with $oxPC_{CD36}$, facilitating their recognition and phagocytosis (*17*−*19*). However, the structural underpinnings of how the macrophage scavenger receptor CD36 recognizes structurally specific oxidized phospholipids within cell membranes or lipoprotein surfaces remained unclear. These studies suggest that lipid oxidation, which occurs during cellular senescence, apoptosis, or lipoprotein aging and/or modification, is accompanied by the reorienting of certain oxidized *sn*-2 fatty acids on surface phospholipids such that their "buoyant" oxygenated terminal ends protrude into the aqueous compartment. The conformation of $oxPC_{CD36}$ within membrane bilayers thus orients the structural motif that confers high-affinity CD36 recognition on the aqueous phase. Evolution has apparently exploited this structure so that it serves as a molecular "tag" on the surface of oxidatively modified cell membranes and lipoproteins for triggering CD36-mediated macrophage recognition and phagocytosis. These results provide new structural insights into potential conformational alterations in membrane phospholipids that occur concurrently with membrane peroxidation associated with cellular senescence or apoptosis in general and, more specifically, for CD36−lipid ligand interactions during innate host defense processes. They also provide a platform for the rational development of potential therapeutic strategies for blocking macrophage recognition of oxidized lipoproteins and foam cell formation.

ACKNOWLEDGMENT

We thank Xian Mao and Dale Ray for technical assistance.

REFERENCES

1. Cohen, J. J. (1991) Programmed cell death in the immune system, *Adv. Immunol. 50*, 55−85.
2. Henson, P. M., Bratton, D. L., and Fadok, V. A. (2001) Apoptotic cell removal, *Curr. Biol. 11*, R795−R805.
3. Savill, J., and Fadok, V. (2000) Corpse clearance defines the meaning of cell death, *Nature 407*, 784−788.
4. Savill, J. S., Wyllie, A. H., Henson, J. E., Walport, M. J., Henson, P. M., and Haslett, C. (1989) Macrophage phagocytosis of aging neutrophils in inflammation. Programmed cell death in the neutrophil leads to its recognition by macrophages, *J. Clin. Invest. 83*, 865−875.
5. Stuart, L. M., and Ezekowitz, R. A. (2005) Phagocytosis: Elegant complexity, *Immunity 22*, 539−550.
6. Endemann, G., Stanton, L. W., Madden, K. S., Bryant, C. M., White, R. T., and Protter, A. A. (1993) CD36 is a receptor for oxidized low density lipoprotein, *J. Biol. Chem. 268*, 11811−18116.
7. Febbraio, M., Hajjar, D. P., and Silverstein, R. L. (2001) CD36: A class B scavenger receptor involved in angiogenesis, atherosclerosis, inflammation, and lipid metabolism, *J. Clin. Invest. 108*, 785−791.
8. Lauber, K., Blumenthal, S. G., Waibel, M., and Wesselborg, S. (2004) Clearance of apoptotic cells: Getting rid of the corpses, *Mol. Cell 14*, 277−287.
9. Lusis, A. J. (2000) Atherosclerosis, *Nature 407*, 233−241.
10. Rigotti, A., Acton, S. L., and Krieger, M. (1995) The class B scavenger receptors SR-BI and CD36 are receptors for anionic phospholipids, *J. Biol. Chem. 270*, 16221−16224.
11. Suzuki, H., Kurihara, Y., Takeya, M., Kamada, N., Kataoka, M., Jishage, K., Ueda, O., Sakaguchi, H., Higashi, T., Suzuki, T., Takashima, Y., Kawabe, Y., Cynshi, O., Wada, Y., Honda, M., Kurihara, H., Aburatani, H., Doi, T., Matsumoto, A., Azuma, S., Noda, T., Toyoda, Y., Itakura, H., Yazaki, Y., Kodama, T., et al. (1997) A role for macrophage scavenger receptors in atherosclerosis and susceptibility to infection, *Nature 386*, 292−296.
12. Febbraio, M., Abumrad, N. A., Hajjar, D. P., Sharma, K., Cheng, W., Pearce, S. F., and Silverstein, R. L. (1999) A null mutation in murine CD36 reveals an important role in fatty acid and lipoprotein metabolism, *J. Biol. Chem. 274*, 19055−19062.
13. Nozaki, S., Kashiwagi, H., Yamashita, S., Nakagawa, T., Kostner, B., Tomiyama, Y., Nakata, A., Ishigami, M., Miyagawa, J., Kameda-Takemura, K., et al. (1995) Reduced uptake of oxidized low density lipoproteins in monocyte-derived macrophages from CD36-deficient subjects, *J. Clin. Invest. 96*, 1859−1865.
14. Ren, Y., Silverstein, R. L., Allen, J., and Savill, J. (1995) CD36 gene transfer confers capacity for phagocytosis of cells undergoing apoptosis, *J. Exp. Med. 181*, 1857−1862.
15. Febbraio, M., Podrez, E. A., Smith, J. D., Hajjar, D. P., Hazen, S. L., Hoff, H. F., Sharma, K., and Silverstein, R. L. (2000) Targeted disruption of the class B scavenger receptor CD36 protects against atherosclerotic lesion development in mice, *J. Clin. Invest. 105*, 1049−1056.
16. Yamashita, S., Hirano, K. I., Kuwasako, T., Janabi, M., Toyama, Y., Ishigami, M., and Sakai, N. (2006) Physiological and pathological roles of a multi-ligand receptor CD36 in atherogenesis: Insights from CD36-deficient patients, *Mol. Cell. Biochem.* (in press).
17. Podrez, E. A., Poliakov, E., Shen, Z., Zhang, R., Deng, Y., Sun, M., Finton, P. J., Shan, L., Febbraio, M., Hajjar, D. P., Silverstein, R. L., Hoff, H. F., Salomon, R. G., and Hazen, S. L. (2002) A novel family of atherogenic oxidized phospholipids promotes macrophage foam cell formation via the scavenger receptor CD36 and is enriched in atherosclerotic lesions, *J. Biol. Chem. 277*, 38517−38523.
18. Podrez, E. A., Poliakov, E., Shen, Z., Zhang, R., Deng, Y., Sun, M., Finton, P. J., Shan, L., Gugiu, B., Fox, P. L., Hoff, H. F., Salomon, R. G., and Hazen, S. L. (2002) Identification of a novel family of oxidized phospholipids that serve as ligands for the macrophage scavenger receptor CD36, *J. Biol. Chem. 277*, 38503−38516.
19. Sun, M., Finnemann, S. C., Febbraio, M., Shan, L., Annangudi, S. P., Podrez, E. A., Hoppe, G., Darrow, R., Organisciak, D. T., Salomon, R. G., Silverstein, R. L., and Hazen, S. L. (2006) Light-induced oxidation of photoreceptor outer segment phospholipids generates ligands for CD36-mediated phagocytosis by retinal pigment epithelium: A potential mechanism for modulating outer segment phagocytosis under oxidant stress conditions, *J. Biol. Chem. 281*, 4222−4230.
20. Greenberg, M. E., Sun, M., Zhang, R., Febbraio, M., Silverstein, R., and Hazen, S. L. (2006) Oxidized phosphatidylserine−CD36 interactions play an essential role in macrophage dependent phagocytosis of apoptotic cells, *J. Exp. Med. 203*, 2613−2625.
21. Rahaman, S. O., Lennon, D. J., Febbraio, M., Podrez, E. A., Hazen, S. L., and Silverstein, R. L. (2006) A CD36-dependent signaling cascade is necessary for macrophage foam cell formation, *Cell Metab. 4*, 211−221.
22. Maxfield, F. R., and Tabas, I. (2005) Role of cholesterol and lipid organization in disease, *Nature 438*, 612−621.
23. Baber, J., Ellena, J. F., and Cafiso, D. S. (1995) Distribution of general anesthetics in phospholipid bilayers determined using ^{2}H NMR and ^{1}H-^{1}H NOE spectroscopy, *Biochemistry 34*, 6533−6539.
24. Ellena, J. F., Dominey, R. N., Archer, S. J., Xu, Z. C., and Cafiso, D. S. (1987) Localization of hydrophobic ions in phospholipid bilayers using ^{1}H nuclear Overhauser effect spectroscopy, *Biochemistry 26*, 4584−4592.
25. Gawrisch, K., Eldho, N. V., and Polozov, I. V. (2002) Novel NMR tools to study structure and dynamics of biomembranes, *Chem. Phys. Lipids 116*, 135−151.
26. Halladay, H. N., Stark, R. E., Ali, S., and Bittman, R. (1990) Magic-angle spinning NMR studies of molecular organization in multibilayers formed by 1-octadecanoyl-2-decanoyl-*sn*-glycero-3-phosphocholine, *Biophys. J. 58*, 1449−1461.
27. Han, X. L., and Gross, R. W. (1990) Plasmenylcholine and phosphatidylcholine membrane bilayers possess distinct conformational motifs, *Biochemistry 29*, 4992−4996.
28. Holte, L. L., and Gawrisch, K. (1997) Determining ethanol distribution in phospholipid multilayers with MAS-NOESY spectra, *Biochemistry 36*, 4669−4674.
29. Xu, Z. C., and Cafiso, D. S. (1986) Phospholipid packing and conformation in small vesicles revealed by two-dimensional ^{1}H nuclear magnetic resonance cross-relaxation spectroscopy, *Biophys. J. 49*, 779−783.
30. Zhou, Z., Sayer, B. G., Hughes, D. W., Stark, R. E., and Epand, R. M. (1999) Studies of phospholipid hydration by high-resolution magic-angle spinning nuclear magnetic resonance, *Biophys. J. 76*, 387−399.
31. Delaglio, F., Grzesiek, S., Vuister, G. W., Zhu, G., Pfeifer, J., and Bax, A. (1995) NMRPipe: A multidimensional spectral processing system based on UNIX pipes, *J. Biomol. NMR 6*, 277−293.
32. Wagner, G., and Wüthrich, K. (1979) Truncated driven nuclear overhauser effect (TOE). A new technique for studies of selective ^{1}H-^{1}H Overhauser effects in the presence of spin diffusion, *J. Magn. Reson. 26*, 629−633.
33. Shimada, H., Grutzner, J. B., Kozlowski, J. F., and McLaughlin, J. L. (1998) Membrane conformations and their relation to cytotoxicity of asimicin and its analogues, *Biochemistry 37*, 854−866.
34. Pace, R. J., and Chan, S. I. (1982) Molecular motions in lipid bilayers. III. Lateral and transverse diffusion in bilayers, *J. Chem. Phys. 76*, 4241−4247.
35. Clore, G. M., and Gronenborn, A. M. (1985) Assessment of errors involves in the determination of interproton distance rations and distances by means of one- and two-dimensional NOE measurements, *J. Magn. Reson. 61*, 158−164.
36. Yau, W. M., and Gawrisch, K. (2000) Lateral lipid diffusion dominates NOESY cross-relaxation in membranes, *J. Am. Chem. Soc. 122*, 3971−3972.
37. Kornberg, R. D., and McConnell, H. M. (1971) Lateral diffusion of phospholipids in a vesicle membrane, *Proc. Natl. Acad. Sci. U.S.A. 68*, 2564−2568.
38. Yeagle, P. L., Hutton, W. C., Huang, C. H., and Martin, R. B. (1975) Headgroup conformation and lipid−cholesterol association in phosphatidylcholine vesicles: A ^{31}P(^{1}H) nuclear Overhauser effect study, *Proc. Natl. Acad. Sci. U.S.A. 72*, 3477−3481.
39. Kouroda, Y., and Kitamura, K. (1984) Intra- and intermolecular ^{1}H-^{1}H nuclear Overhauser effect studies on the interactions of chlorpromazine with lecithin vesicles, *J. Am. Chem. Soc. 106*, 1−6.
40. Tilcock, C. P., and Cullis, P. R. (1987) Lipid polymorphism, *Ann. N.Y. Acad. Sci. 492*, 88−102.

41. Cullis, P. R., and de Kruijff, B. (1979) Lipid polymorphism and the functional roles of lipids in biological membranes, *Biochim. Biophys. Acta 559*, 399−420.
42. Funari, S. S., Nuscher, B., Rapp, G., and Beyer, K. (2001) Detergent-phospholipid mixed micelles with a crystalline phospholipid core, *Proc. Natl. Acad. Sci. U.S.A. 98*, 8938−8943.
43. Kooijman, E. E., Carter, K. M., van Laar, E. G., Chupin, V., Burger, K. N., and de Kruijff, B. (2005) What makes the bioactive lipids phosphatidic acid and lysophosphatidic acid so special? *Biochemistry 44*, 17007−17015.
44. Lohner, K., Staudegger, E., Prenner, E. J., Lewis, R. N., Kriechbaum, M., Degovics, G., and McElhaney, R. N. (1999) Effect of staphylococcal δ-lysin on the thermotropic phase behavior and vesicle morphology of dimyristoylphosphatidylcholine lipid bilayer model membranes. Differential scanning calorimetric, ^{31}P nuclear magnetic resonance and Fourier transform infrared spectroscopic, and X-ray diffraction studies, *Biochemistry 38*, 16514−16528.
45. Traikia, M., Warschawski, D. E., Recouvreur, M., Cartaud, J., and Devaux, P. F. (2000) Formation of unilamellar vesicles by repetitive freeze-thaw cycles: Characterization by electron microscopy and ^{31}P-nuclear magnetic resonance, *Eur. Biophys. J. 29*, 184−195.
46. Wüthrich, K. (2003) NMR studies of structure and function of biological macromolecules, *Biosci. Rep. 23*, 119−168.
47. Pearson, R. H., and Pascher, I. (1979) The molecular structure of lecithin dihydrate, *Nature 281*, 499−501.
48. Buldt, G., Gally, H. U., Seelig, A., Seelig, J., and Zaccai, G. (1978) Neutron diffraction studies on selectively deuterated phospholipid bilayers, *Nature 271*, 182−184.
49. Bechinger, B., and Seelig, J. (1991) Interaction of electric dipoles with phospholipid head groups. A ^{2}H and ^{31}P NMR study of phloretin and phloretin analogues in phosphatidylcholine membranes, *Biochemistry 30*, 3923−3929.
50. Hauser, H., Pascher, I., Pearson, R. H., and Sundell, S. (1981) Preferred conformation and molecular packing of phosphatidylethanolamine and phosphatidylcholine, *Biochim. Biophys. Acta 650*, 21−51.
51. Seelig, J., Gally, G. U., and Wohlgemuth, R. (1977) Orientation and flexibility of the choline head group in phosphatidylcholine bilayers, *Biochim. Biophys. Acta 467*, 109−119.
52. Singer, S. J., and Nicolson, G. L. (1972) The fluid mosaic model of the structure of cell membranes, *Science 175*, 720−731.

BI700163Y